PNAS PLUS

IL-33 ameliorates Alzheimer's disease-like pathology and cognitive decline

Amy K. Y. Fu[a,b,c], Kwok-Wang Hung[a,b,c], Michael Y. F. Yuen[a,b,c], Xiaopu Zhou[a,b,c], Deejay S. Y. Mak[a,b,c], Ivy C. W. Chan[a,b,c], Tom H. Cheung[a,b,c], Baorong Zhang[d], Wing-Yu Fu[a,b,c], Foo Y. Liew[e,f,1], and Nancy Y. Ip[a,b,c,1]

[a]Division of Life Science, The Hong Kong University of Science and Technology, Hong Kong, China; [b]Molecular Neuroscience Center, The Hong Kong University of Science and Technology, Hong Kong, China; [c]State Key Laboratory of Molecular Neuroscience, The Hong Kong University of Science and Technology, Hong Kong, China; [d]Department of Neurology, The Second Affiliated Hospital, School of Medicine, Zhejiang University, Hangzhou, Zhejiang 310009, China; [e]Institute of Infection, Immunity, and Inflammation, College of Medical, Veterinary, and Life Sciences, University of Glasgow, Glasgow G12 8TA, United Kingdom; and [f]School of Biology and Basic Medical Sciences, Soochow University, Suzhou 215006, China

Contributed by Nancy Y. Ip, March 15, 2016 (sent for review February 6, 2016; reviewed by David Morgan and Luke A. J. O'Neill)

Alzheimer's disease (AD) is a devastating condition with no known effective treatment. AD is characterized by memory loss as well as impaired locomotor ability, reasoning, and judgment. Emerging evidence suggests that the innate immune response plays a major role in the pathogenesis of AD. In AD, the accumulation of β-amyloid (Aβ) in the brain perturbs physiological functions of the brain, including synaptic and neuronal dysfunction, microglial activation, and neuronal loss. Serum levels of soluble ST2 (sST2), a decoy receptor for interleukin (IL)-33, increase in patients with mild cognitive impairment, suggesting that impaired IL-33/ST2 signaling may contribute to the pathogenesis of AD. Therefore, we investigated the potential therapeutic role of IL-33 in AD, using transgenic mouse models. Here we report that IL-33 administration reverses synaptic plasticity impairment and memory deficits in APP/PS1 mice. IL-33 administration reduces soluble Aβ levels and amyloid plaque deposition by promoting the recruitment and Aβ phagocytic activity of microglia; this is mediated by ST2/p38 signaling activation. Furthermore, IL-33 injection modulates the innate immune response by polarizing microglia/macrophages toward an antiinflammatory phenotype and reducing the expression of proinflammatory genes, including IL-1β, IL-6, and NLRP3, in the cortices of APP/PS1 mice. Collectively, our results demonstrate a potential therapeutic role for IL-33 in AD.

innate immunity | synaptic plasticity | β-amyloid | microglia | neuroninflammation

Alzheimer's disease (AD) is the most common type of dementia in the elderly population, and its prevalence is increasing with the rapidly growing global elderly population (1). AD is characterized by progressive memory loss and other cognitive dysfunctions, such as impaired locomotor ability, reasoning, and judgment (2, 3). The hallmarks of AD pathology include the presence of extracellular amyloid plaque deposits, composed of Aβ peptides, and the intracellular formation of neurofibrillary tangles in the brain, together with synaptic dysfunction and neuronal loss.

The mechanisms underlying the onset and progression of AD remain unclear. Mutations of amyloid precursor protein and presenilins that result in abnormal production of Aβ peptides are suggested to play a dominant role in the pathogenesis of early-onset familial AD (4). Identification of several innate response genes in genome-wide association studies support the idea that innate immunity is involved in the more common sporadic late-onset form of AD (LOAD) (4).

Studies of transgenic mouse models of AD suggest the impairment of microglial function to reduce Aβ burden as a causal factor in the disease (5). Specifically, in AD, microglial activation attempts to eliminate Aβ accumulation by enhancing Aβ phagocytosis, clearance, and degradation; however, the continuous generation and aberrant accumulation of Aβ in the brain causes microglial dysfunction by reducing Aβ receptors and increasing the generation of inflammatory mediators (5). Chronic neuroinflammation induced by microglia contributes to pathological progression and symptom severity in late stages of the disease. Importantly, although sometimes contradictory, modulation of the immune system by specific interleukin signals such as IL-12/IL-23 and IL-10, as well as the inflammasome pathway, ameliorates AD-like pathology (6–9).

IL-33, an alarmin of the IL-1 family, is a crucial mediator of the innate immune response and a regulator of immune cell infiltration and activation (10). IL-33 is expressed in various cell types (10, 11). IL-33 binds to a heterodimeric receptor complex, comprising ST2 and IL-1RAcP, and triggers the intracellular cascade involve myeloid differentiation factor 88 (MyD88) and NF-κB. This signaling selectively activates type 2 T-helper cells, mast cells, neutrophils, and alternatively-activated macrophages (10). In the central nervous system (CNS), IL-33 is constitutively expressed in oligodendrocytes (12), whereas ST2 is expressed mainly in microglia and astrocytes (13). IL-33 is a pleiotropic cytokine with diverse functions in various infectious and inflammatory diseases that may exert beneficial or detrimental effects on the disease (10, 14). Genetic studies have identified three single nucleotide polymorphisms in the IL-33 gene that are associated with a reduced risk of AD development (15). IL-33 transcript levels are decreased in the brains of LOAD cases (15). How IL-33 is involved in the pathogenesis of AD, in particular

Significance

Dysfunction of the innate immune system is involved in the pathogenesis of Alzheimer's disease (AD); however, the pathophysiological mechanisms underlying these dysfunctions are unclear. Here we report that stimulation of IL-33/ST2 signaling rescues memory deficits and reduces the accumulation of β-amyloid in APP/PS1 mice that exhibit select pathologies associated with AD. Although impaired IL-33/ST2 signaling is associated with early progression of AD, IL-33 injection rescues contextual memory deficits and reduces the accumulation of β-amyloid in APP/PS1 mice. IL-33 skews the microglia toward an alternative activation state with enhanced Aβ phagocytic capacity and elevated antiinflammatory gene expression, which results in a decreased proinflammatory response in the brain. Thus, this study suggests that IL-33 can be developed as a new therapeutic intervention for AD.

Author contributions: A.K.Y.F., K.-W.H., M.Y.F.Y., W.-Y.F., F.Y.L., and N.Y.I. designed research; K.-W.H., M.Y.F.Y., X.Z., D.S.Y.M., and I.C.W.C. performed research; T.H.C., B.Z., F.Y.L., and N.Y.I. contributed new reagents/analytic tools; A.K.Y.F., K.-W.H., M.Y.F.Y., W.-Y.F., F.Y.L., and N.Y.I. analyzed data; and A.K.Y.F., W.-Y.F., F.Y.L., and N.Y.I. wrote the paper.

Reviewers: D.M., University of South Florida; and L.A.J.O., Trinity College.

The authors declare no conflict of interest.

Freely available online through the PNAS open access option.

[1]To whom correspondence may be addressed. Email: foo.liew@glasgow.ac.uk or boip@ust.hk.

This article contains supporting information online at www.pnas.org/lookup/suppl/doi:10.1073/pnas.1604032113/-/DCSupplemental.

whether replenishment of IL-33 can alleviate AD pathology, remains unclear, however.

Here we show that IL-33 treatment reverses synaptic plasticity and cognitive deficits in APP/PS1 mice, an AD mouse model that exhibits selected pathologies of AD, including amyloid plaque deposition and cognitive impairment. IL-33 reduces soluble Aβ and amyloid plaque load by promoting the recruitment and phagocytic activity of microglia. Furthermore, IL-33 injection modulates the immune response of APP/PS1 mice and polarizes microglia/macrophages toward an antiinflammatory phenotype. Collectively, our results demonstrate the potential therapeutic role of IL-33 in AD.

Results

IL-33 transcript and protein levels are reportedly lower in the brains of patients with LOAD compared with brains of healthy individuals (15). We found significantly higher levels of serum sST2, a decoy receptor of IL-33, in patients with mild cognitive impairment (MCI; with an increased risk of developing to AD in later life) compared with healthy controls (Fig. 1*A*); however, whether and how IL-33 is involved in AD pathogenesis, specifically whether replenishment of IL-33 can alleviate AD pathology, remain unclear. Therefore, we used the APPswePS1de9 (hereinafter designated APP/PS1) transgenic mouse model of amyloid plaque deposition (16) to examine the effect of IL-33 on amyloid pathology.

First, we investigated whether increasing IL-33 levels can rescue hippocampal synaptic plasticity impairment and cognitive deficits in APP/PS1 mice. Whereas high-frequency stimulation significantly increased the magnitude of long-term potentiation (LTP) at Schaffer collateral (SC)-CA1 synapses in the hippocampus of wild type (WT) mice, LTP was significantly impaired in 6- to 7-mo-old APP/PS1 mice (17, 18). An i.p. injection of recombinant IL-33 (200 ng) for 2 d dramatically reversed the LTP impairment of APP/PS1 mice (Fig. 1 *B* and *C*).

We next assessed the effect of IL-33 on modulating the behavioral performance of the APP/PS1 mice. In the exploratory

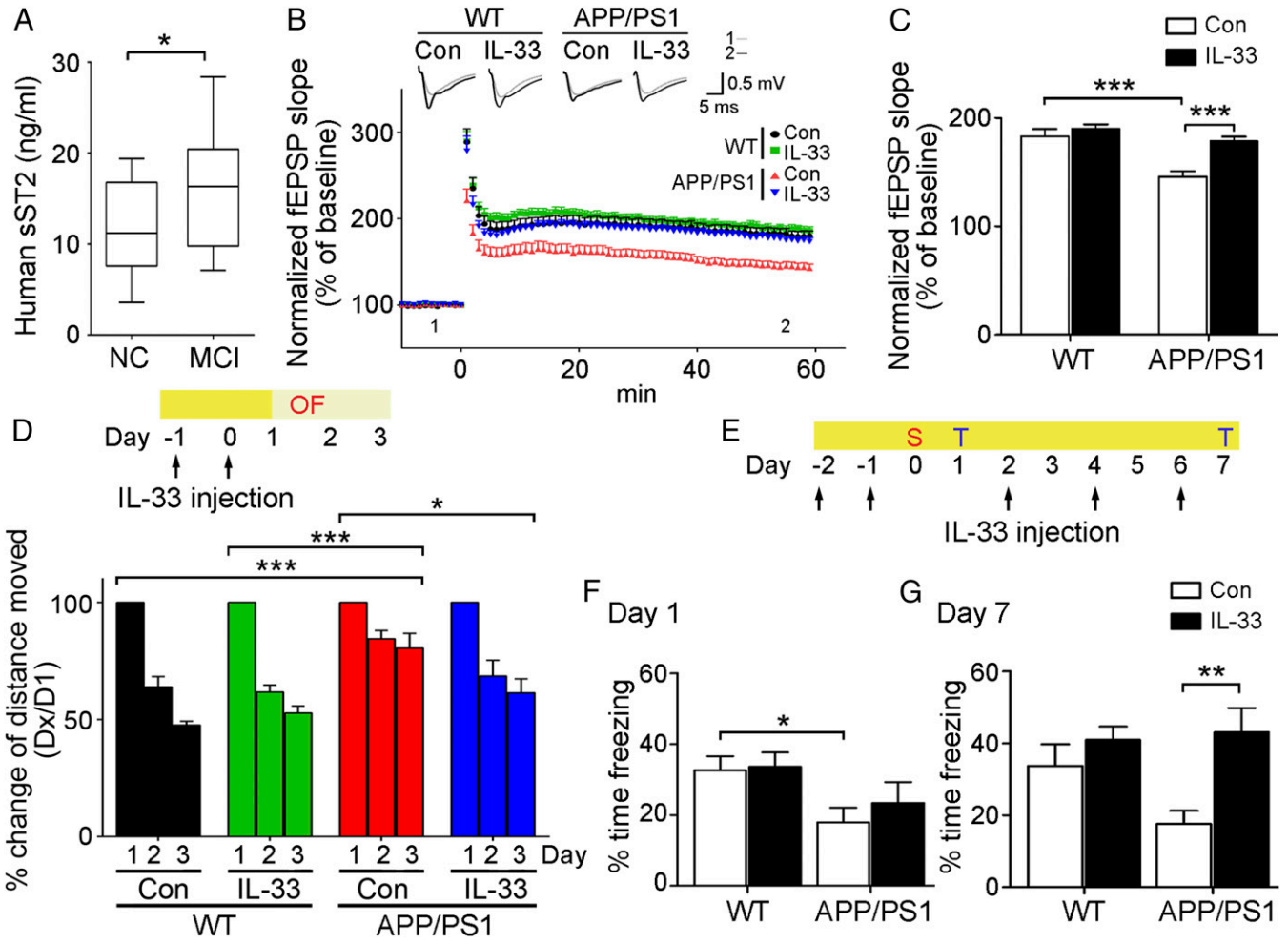

Fig. 1. IL-33 administration ameliorates synaptic impairment and behavioral deficits in APP/PS1 mice. (*A*) Boxplot showing the sST2 levels in the serum of healthy subjects (NC; $n = 17$) and patients with MCI ($n = 18$). *$P < 0.05$, two-sample t test. (*B* and *C*) IL-33 rescues LTP impairment in APP/PS1 mutant mice. WT and APP/PS1 mice at age 6 to 7 mo were given IL-33 or vehicle control (Con). LTP in the hippocampal CA1 region was induced by high-frequency stimulation (HFS). (*B*) Averaged slopes of baseline normalized fEPSP (mean ± SEM). (*Inset*) Examples of fEPSPs recorded 5 min before (1, gray) and 55 min after (2, black) LTP induction. (*C*) Quantification of mean fEPSP slopes during the last 10 min of the recording after LTP induction. $n = 16$–18 slices from eight mice, representative of three experiments. ***$P < 0.001$, two-way ANOVA with Bonferroni post hoc test. (*D*) IL-33–treated APP/PS1 mice (14 mo old) exhibit improved habituation in the exploratory open field (OF) test. (*Upper*) Timeline of IL-33 administration and the OF test. (*Lower*) Percentage change in distance traveled relative to the distance traveled on the first day of training. $n = 11$–13 mice/group. Data are mean ± SEM. *$P < 0.05$; ***$P < 0.001$, two-way repeated-measures ANOVA. (*E*–*G*) IL-33 ameliorates memory retrieval deficits of APP/PS1 mice in fear conditioning (FC) tests. (*E*) Timeline of IL-33 administration and FC test. S, electrical shock; T, freezing tests. The graphs show the percentage of freezing time after 1 d (*F*) and 7 d (*G*) of electric shocks. $n = 11$–13 mice/group. Data are mean ± SEM. *$P < 0.05$; **$P < 0.01$, two-way ANOVA with Bonferroni post hoc test.

open field test, the vehicle-injected and IL-33–injected WT mice exhibited similar habituation ability in novel testing environments during the 3-d training course (Fig. 1*D* and *SI Appendix*, Fig. S1). The APP/PS1 mice exhibited significantly slower habituation to the testing environment than the WT mice; however, the IL-33–treated APP/PS1 mice showed significantly improved habituation to the testing environment (Fig. 1*D* and *SI Appendix*, Fig. S1).

We also assessed the memory formation and retrieval abilities of the IL-33–treated APP/PS1 mice using the contextual fear-conditioning test, by evaluating their freezing response at 1 d and 7 d after the administration of electric shock (Fig. 1 *E*–*G*). The mice of different experimental groups did not exhibit any significant difference in freezing response immediately after electric shock (*SI Appendix*, Fig. S2). Compared with the WT mice, the APP/PS1 mice exhibited reduced freezing behavior at 1 d and 7 d after the electric shock, indicating an impaired contextual retrieval of fear memory (Fig. 1 *F* and *G*). Whereas the IL-33–treated APP/PS1 mice did not exhibit an improvement in freezing performance 1 d after the electric shock (Fig. 1*F*), IL-33 treatment was able to restore the impaired freezing response of the APP/PS1 mice at 7 d after the electric shock (Fig. 1*G*). These data suggest that IL-33 treatment reverses contextual memory deficits in APP/PS1 mice, probably through ameliorating the hippocampal synaptic dysfunctions.

IL-33 reached the brain within 30 min after i.p. injection (*SI Appendix*, Fig. S3), consistent with earlier findings of a compromised blood–brain barrier in both APP/PS1 mice and patients with AD (19, 20). At the concentration used (200 ng i.p. daily for 2 d), IL-33 did not affect the general health or plasma histamine level in either WT or APP/PS1 mice (*SI Appendix*, Fig. S4). Collectively, these results demonstrate that IL-33 can rescue the synaptic dysfunction and memory deficits of APP/PS1 mice.

We then investigated whether IL-33 administration exerts a beneficial effect on the pathological conditions of AD by measuring soluble Aβ levels and amyloid plaque deposition in APP/PS1 mice. Western blot analysis showed that IL-33 injection significantly reduced the amounts of soluble Aβ in the cortices of 10-mo-old (by 54 ± 9%, $n = 3$ experiments; Fig. 2*A*) and 25-mo-old (*SI Appendix*, Fig. S5) APP/PS1 mice. Specifically, soluble $A\beta_{x-40}$ and $A\beta_{x-42}$ species, which play major synaptotoxic roles in AD (21), were decreased by ∼50% and ∼30%, respectively, in the cortices of 10-mo-old IL-33–administered APP/PS1 mice (Fig. 2*B*). At 2 d after IL-33 treatment, the 4G8-labeled amyloid plaques were significantly reduced in the cortices of 12-mo-old APP/PS1 mice (Fig. 2 *C* and *D*). Importantly, intracerebroventricular administration of sST2 abolished the IL-33–mediated reduction of 4G8-stained amyloid plaques in the APP/PS1 mice (Fig. 2 *C* and *D*), demonstrating the specificity and the central activation

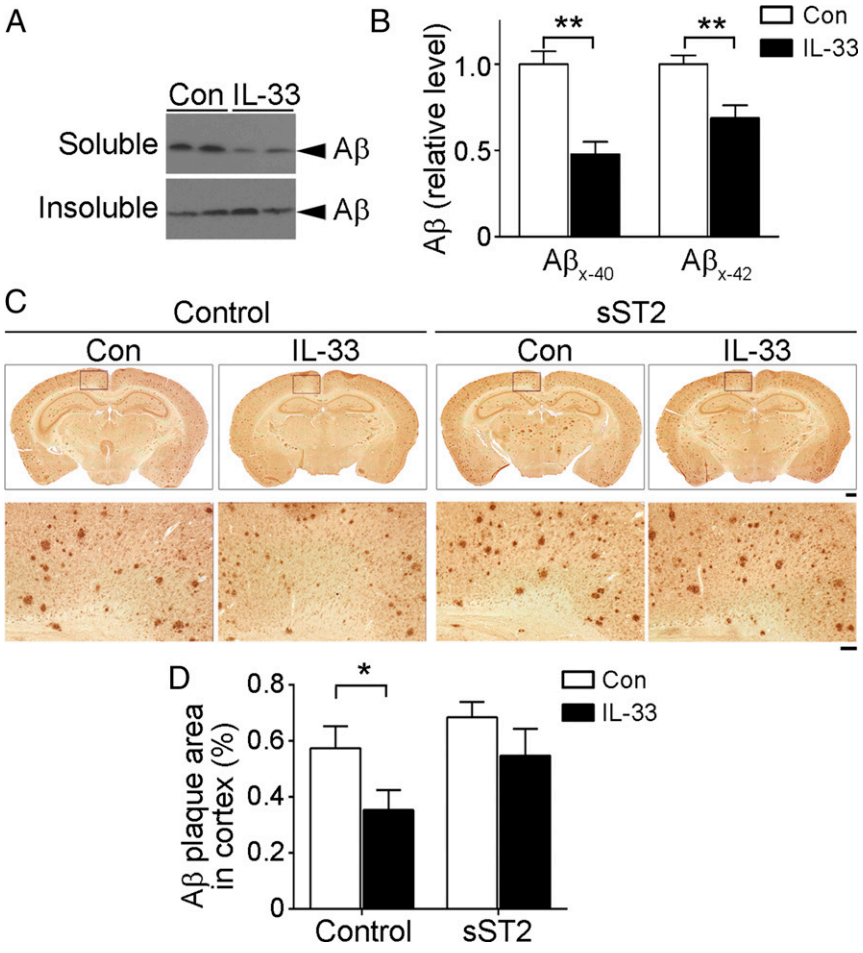

Fig. 2. IL-33 administration reduces soluble Aβ levels and Aβ plaques in APP/PS1 mice. (*A*) IL-33 reduced soluble Aβ content. Representative Western blot of soluble and insoluble Aβ in cortical homogenates of 10-mo-old APP/PS1 mice. $n = 6$ mice from three experiments. (*B*) Quantitative analysis of relative $A\beta_{x-40}$ and $A\beta_{x-42}$ levels in soluble fractions of APP/PS1 mice measured by ELISA. $n = 4$ mice per group. $^{**}P < 0.01$, Student's t test. (*C* and *D*) IL-33 ameliorated amyloid plaque pathology in APP/PS1 mice. Representative images (*C*) and quantification (*D*) of 4G8-stained amyloid plaques in the cortices of APP/PS1 mice (12 mo old) after IL-33 administration with or without sST2 infusion. $n = 7$ mice/group. $^{*}P < 0.05$, one-way ANOVA with Bonferroni post hoc test. All data are mean ± SEM. (Scale bars: *Top*, 500 μm; *Bottom*, 100 μm.)

of myeloid cells of IL-33/ST2 signaling in ameliorating the cerebral amyloid pathology. IL-33 administration for 2 d also reduced 4G8-stained amyloid plaques in 5XFAD mice, another AD transgenic mouse model (*SI Appendix*, Fig. S6).

Because the Aβ phagocytic activity of microglia directly impacts Aβ clearance (22, 23), we examined whether Aβ phagocytosis and degradation by resident microglia/infiltrating monocytes are altered in APP/PS1 mouse brains following IL-33 administration. To mediate Aβ phagocytic uptake, myeloid cells are first recruited to amyloid plaques before being activated and phagocytosing Aβ (8, 24). Clusters of Iba1$^+$ myeloid cells were found adjacent to the amyloid plaques in the cortices of the APP/PS1 mice (Fig. 3*A*). IL-33 injection enhanced the recruitment of Iba1$^+$ myeloid cells to amyloid plaques in these cortices (Fig. 3*A*). Our 3D analysis confirmed the increased colocalization of myeloid cells and amyloid plaques in IL-33–treated APP/PS1 mouse brains (Fig. 3 *B* and *C*), supporting the notion that IL-33 enhances the proximity between myeloid cells and amyloid plaques.

CD68, a transmembrane glycoprotein of the lysosomal/endosomal-associated membrane glycoprotein family, acts as a scavenger receptor for debris clearance (25, 26). In APP/PS1 mice, the clusters of Iba1$^+$ myeloid cells surrounding amyloid plaques exhibited diffuse CD68 distribution (Fig. 3*D*). IL-33 administration increased CD68 expression in Iba1$^+$ myeloid cells, that were in close contact with amyloid plaques (Fig. 3*E*). These findings suggest that IL-33 administration increases phagocytic Aβ uptake by myeloid cells.

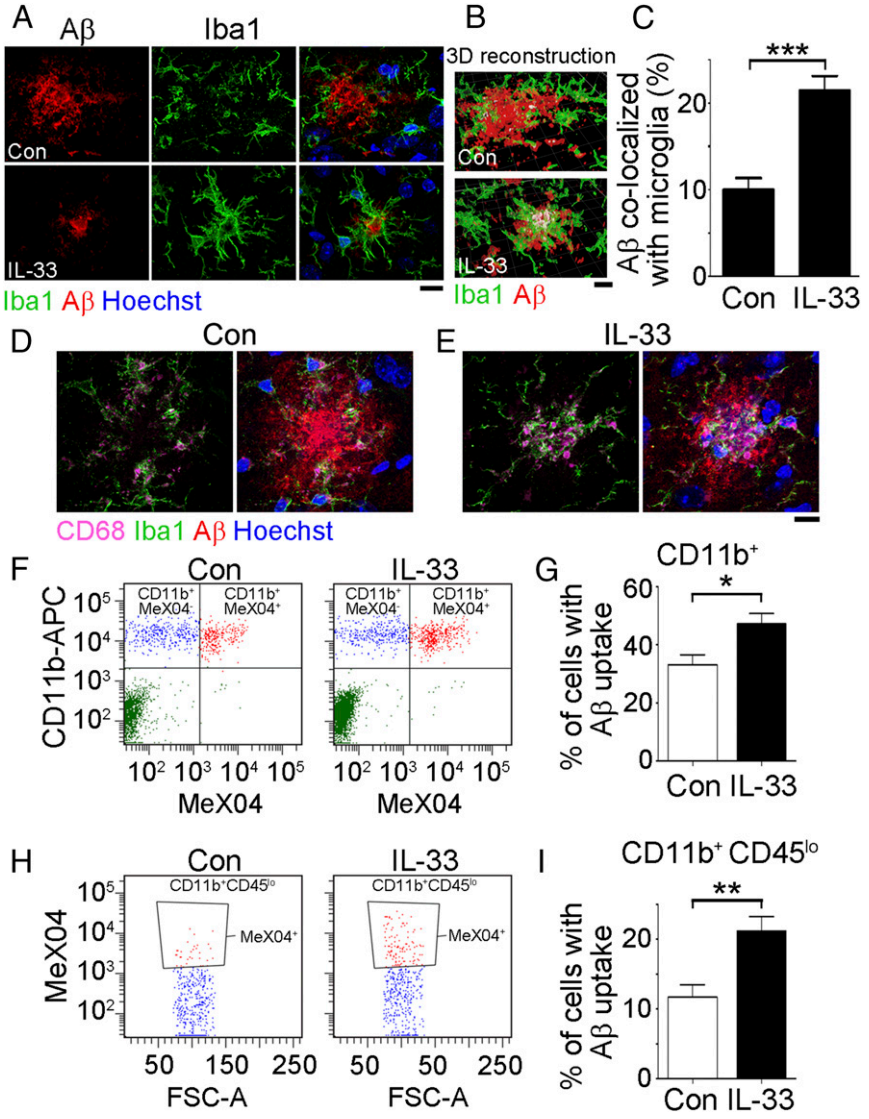

Fig. 3. IL-33 administration enhances microglial phagocytosis of Aβ. (*A*–*C*) IL-33 increases the colocalization of Iba1$^+$ myeloid cells and Aβ plaques in the cortices of APP/PS1 mice (12 mo old). Representative confocal images (*A*) and 3D reconstruction (*B*) show the interaction between Aβ plaques and Iba1$^+$ cells. (*C*) Quantification of the 3D colocalization of Aβ plaques and Iba1$^+$ staining. $n = 16$ images from four mice. ***$P < 0.001$, Student's *t* test. (*D* and *E*) IL-33 increases CD68 expression in Aβ plaques. Representative projected confocal images showing CD68 staining in Iba1$^+$ cells (*Left*) and distribution of CD68$^+$Iba1$^+$ cells around the Aβ plaques (*Right*) in the cortices of vehicle-treated (Con; *D*) or IL-33–treated (*E*) APP/PS1 mice. (*F*–*I*) IL-33 enhances the phagocytic activity of resident microglial cells. Representative scatterplots and quantification show the percentages of CD11b$^+$ mononuclear cells (*F* and *G*) and CD11b$^+$CD45^{lo} cells (*H* and *I*) containing methoxy-X04–labeled Aβ in the APP/PS1 mouse brains (17 mo old) after IL-33 administration. *Top* quadrants (red and blue) in *F* were identified as myeloid cell populations, whereas *Top Right* quadrants in *F* and the gate in *H* represent populations of cells that phagocytosed Aβ [methoxy-X04$^+$ (MeX04$^+$)]. Con, $n = 5$ mice; IL-33, $n = 6$ mice from three experiments. All data are mean ± SEM. *$P < 0.05$; **$P < 0.01$, Student's *t* test. (Scale bars: 10 μm.)

To directly demonstrate that IL-33 promotes Aβ phagocytosis by myeloid cells, we injected APP/PS1 mice with methoxy-X04, a fluorescent dye that crosses the blood-brain barrier and specifically binds Aβ (7). Flow cytometry analysis detected methoxy-X04–labeled Aβ in ∼33% of the CD11b$^+$ myeloid cells from the cortices of the APP/PS1 mice (Fig. 3 *F* and *G*), but not those of WT mice (*SI Appendix*, Fig. S7). IL-33 injection further increased the proportion of CD11b$^+$ cells exhibiting methoxy-X04 fluorescence (∼47%; Fig. 3 *F* and *G*).

Both resident microglia and infiltrating monocytes are suggested to play phagocytic roles in clearing unwanted materials in neurodegeneration and brain injury (27, 28); therefore, we examined the subset(s) of CD11b$^+$ myeloid cells that exhibited increased Aβ phagocytic activity in IL-33–treated APP/PS1 mouse brains. Resident microglia and infiltrated monocytes can be differentiated by low (CD45^{lo}) and high (CD45^{hi}) CD45 expression, respectively (29). We found that most CD11b$^+$ myeloid cells in the WT mice were resident microglia, as characterized by the low CD45 expression (>90% CD45^{lo}; *SI Appendix*, Fig. S8*A*). The APP/PS1 mice exhibited ∼3.6-fold more infiltrating monocytes (CD11b$^+$CD45^{hi} myeloid cells) compared with the WT mice (*SI Appendix*, Fig. S8 *A–D*). In the APP/PS1 mice, ∼10% of CD11b$^+$CD45^{lo} resident microglia phagocytosed Aβ (Fig. 3 *H* and *I*), and ∼80% of CD11b$^+$CD45^{hi} infiltrating monocytes took up the methoxy-X04–labeled Aβ (*SI Appendix*, Fig. S8 *E–G*). IL-33 administration significantly increased Aβ phagocytic uptake by resident microglia by ∼80%, whereas the percentage of Aβ-containing infiltrating monocytes remained relatively stable (Fig. 3 *H* and *I* and *SI Appendix*, Fig. S8 *E–G*). In addition, soluble Aβ can be degraded by Aβ-degrading enzymes, including neprilysin and

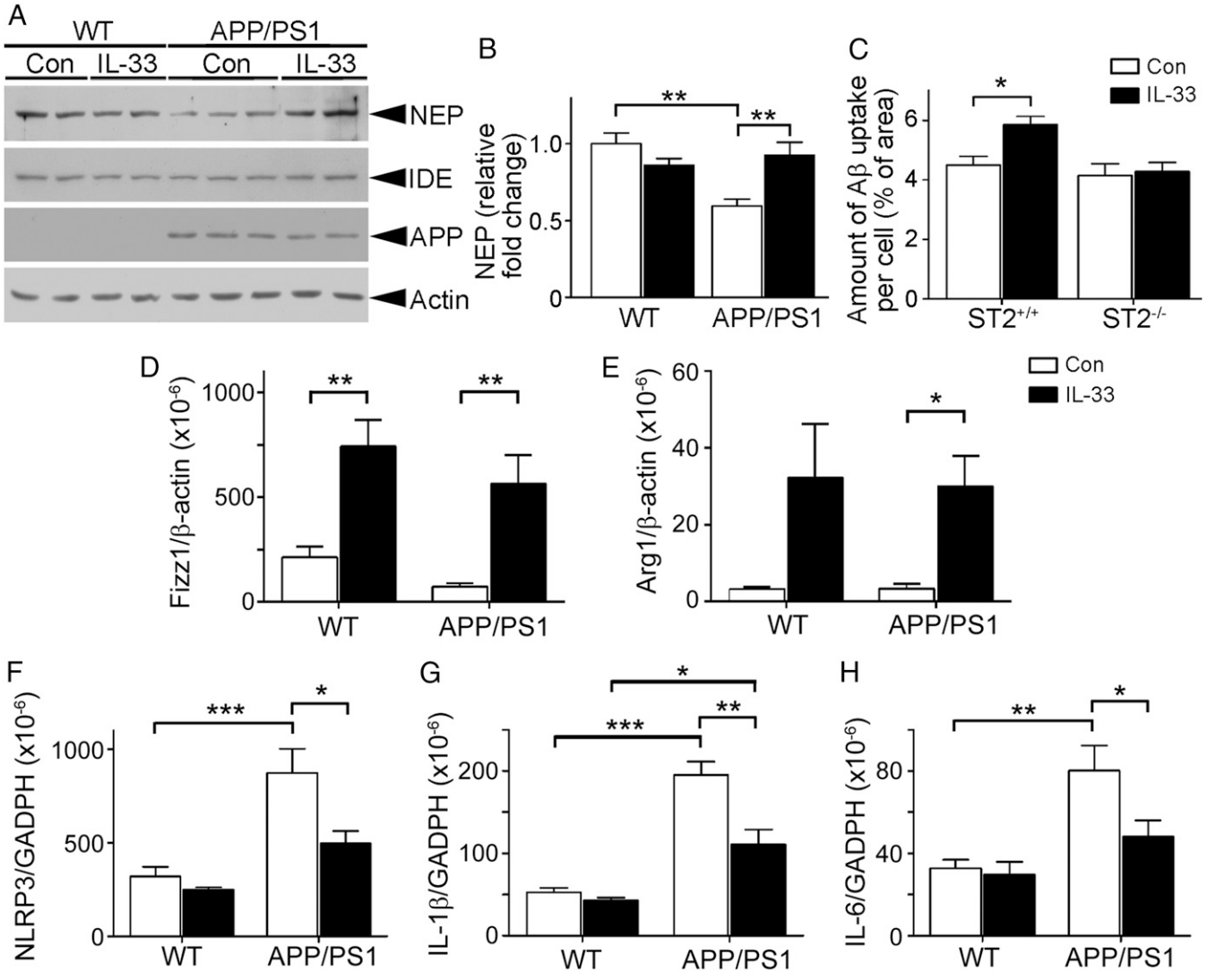

Fig. 4. IL-33 modulates inflammatory responses in APP/PS1 mice. (*A* and *B*) IL-33 administration increases neprilysin protein level in the brains of APP/PS1 mice. WT and APP/PS1 mice (14 mo old) were treated with IL-33 or PBS (Con). Representative Western blot (*A*) and quantification of neprilysin (NEP; *B*) expression are shown. $n = 4$ cortices per group. $^{**}P < 0.01$, two-way ANOVA with Bonferroni post hoc test. (*C*) ST2-deficient microglia abolished the IL-33–stimulated Aβ uptake. Shown are the differences in fluorescein-labeled $A\beta_{1-42}$ uptake between the control (Con) and IL-33–treated primary ST2$^{+/+}$ and ST2$^{-/-}$ adult microglia cultures. $n = 6$ mice in three experiments. $^{*}P < 0.05$, one-way ANOVA with Bonferroni post hoc test. (*D* and *E*) IL-33 drives microglia to an alternative activation state in APP/PS1 mice. Shown is quantitative ddPCR analysis of Fizz1 (*D*) and Arg1 (*E*) mRNA levels in microglia isolated from IL-33–administered APP/PS1 mouse brains. WT/Con, $n = 5$ mice; WT/IL-33, $n = 4$ mice; APP/PS1/Con, $n = 7$ mice; APP/PS1/IL-33, $n = 6$ mice. $^{*}P < 0.05$; $^{**}P < 0.01$, two-way ANOVA with Bonferroni post hoc test. (*F–H*) IL-33 suppresses the proinflammatory genes in APP/PS1 mice. Shown is quantitative ddPCR analysis of NLRP3 (*F*), IL-1β (*G*), and IL-6 (*H*) in the cortices of 12-mo-old APP/PS1 mice. WT/Con, $n = 5$ mice; WT/IL-33, $n = 3$ mice; APP/PS1/Con, $n = 5$ mice; APP/PS1/IL-33, $n = 4$ mice. $^{*}P < 0.05$; $^{**}P < 0.01$; $^{***}P < 0.001$, two-way ANOVA with Bonferroni post hoc test. All data are mean ± SEM.

insulin-degrading enzyme (30). Whereas reduced neprilysin expression was observed in the brains of APP/PS1 mice, IL-33 administration significantly increased neprilysin protein expression, but not insulin-degrading enzyme expression, in APP/PS1 mice (Fig. 4 *A* and *B* and *SI Appendix*, Fig. S9). Taken together, our results demonstrate that IL-33 administration mitigates the amyloid plaque pathology in APP/PS1 mice through the enhancement of Aβ phagocytosis by resident microglia and Aβ clearance, probably by increasing neprilysin levels.

We then examined how IL-33 triggers Aβ uptake by microglial cells. IL-33 enhanced the uptake of fluorescence-labeled oligomeric $A\beta_{1-42}$ in cultured microglial cells in WT mice in a dose-dependent manner (*SI Appendix*, Fig. S10), but not in ST2-deficient microglia (Fig. 4*C*). Concordant with the prominent expression of ST2 in microglia (*SI Appendix*, Fig. S11*A*), the downstream signaling molecules (p38 and ERK1/2 MAPKs) of ST2 receptors were activated in cultured microglia on IL-33 treatment (*SI Appendix*, Fig. S11 *B–D*). These results indicate that ST2 signaling in microglia mediates the IL-33–associated enhancement of Aβ phagocytosis in the brain of APP/PS1 mice.

The inflammatory responses in the brain play a significant role in AD pathology (5, 31). Microglial polarization is associated with the immune response in the CNS (32). Importantly, the mRNA expression of Arg1 and Fizz1, which are associated with antiinflammatory action, was significantly increased in $CD11b^+$ myeloid cells isolated from both WT and APP/PS1 mouse brains after IL-33 administration (Fig. 4 *D* and *E*). These results suggest that IL-33 drives the microglia/macrophages in the APP/PS1 mouse brains toward an alternative activation phenotype, which may contribute to neuroprotective functions. Furthermore, our results suggest that IL-33 can ameliorate global inflammation in the brain cortices of APP/PS1 mice. In the APP/PS1 mice, proinflammatory genes including IL-1β, IL-6, and NLRP3 (NOD-like receptor family, pyrin domain-containing 3, a key component in the inflammasome cascade) were significantly induced in the brain cortex. IL-33 administration significantly suppressed the increased expression of these proinflammatory genes (Fig. 4 *F–H*). Taken together, these findings suggest that IL-33 regulates inflammatory responses in the APP/PS1 mouse brain.

Discussion

There is no effective therapy for AD, in part because of our limited knowledge of its underlying pathophysiological mechanisms. Nonetheless, manipulation of the innate immune system has been considered a promising approach for the development of an effective therapeutic strategy for AD. The present study demonstrates that peripheral IL-33 administration in AD mouse models alleviates AD-like pathology by enhancing microglial phagocytosis and degradation of Aβ. Furthermore, IL-33 treatment switches the microglia/macrophages to an alternative activation phenotype, resulting in a reduction of the proinflammatory response in the AD mouse brains. Considered along with the beneficial effects of IL-33 on synaptic and memory functions in the AD-like mouse model, our results suggest that IL-33 administration can be developed as a potential therapeutic intervention for AD.

IL-33 is a pleiotropic cytokine whose roles depend on inflammation sites and stimulant types. IL-33/ST2 signaling plays a protective role in some diseases caused by sterile inflammation (where the activation of innate immunity is not triggered by infection), such as atherosclerosis and obesity (10, 14). In atherosclerosis, IL-33 reduces atherosclerotic plaque formation by reducing macrophage foam cell formation and increasing production of the antiinflammatory cytokine IL-5 and antioxidized low-density lipoprotein antibody (33, 34). Similarly, Aβ-stimulated sterile inflammation in AD also plays an important role in disease pathogenesis (35). IL-33 expression is reduced in the brains of patients with AD (15), and sST2 is increased in the serum of patients with MCI, as demonstrated in the present study (Fig. 1*A*). These results raise the intriguing possibility that impaired IL-33/ST2 signaling contributes to the nonresolution of sterile inflammation, resulting in amyloid plaque deposition, chronic neuroinflammation, and increased symptom severity in AD. Indeed, our findings show that replenishment of IL-33 is able to reduce the AD-like pathology in the brains of APP/PS1 mice.

What are the underlying mechanisms that mediate the ability of IL-33/ST2 signaling to attenuate AD pathology? Clearance of Aβ is controlled by complex mechanisms, and its dysregulation has been suggested to be a major disease culprit (36). The first responders to Aβ accumulation are the microglia, which are recruited to amyloid plaques. Interestingly, the Aβ-clearing capacity of microglia in APP/PS1 mice is impaired with aging, as revealed by reduced expression of Aβ-binding receptors and Aβ-degrading enzymes (37). In particular, it has been suggested that microglia become inefficient in phagocytosing Aβ during AD progression. IL-33 specifically enhances Aβ uptake by microglia. The increased numbers of $CD68^+$ phagocytic microglial cells around amyloid plaques in APP/PS1 mice after IL-33 treatment suggests that IL-33 is able to restore the phagolysosomal activity of microglia and promote Aβ clearance. Furthermore, treatment of primary adult microglia with IL-33 enhances Aβ uptake, whereas abolishing ST2 expression in microglia reduces this uptake. These findings suggest that IL-33–dependent activation of ST2 signaling in microglia enhances Aβ phagocytosis and clearance. Further phenotypic characterization of this microglial subset that exhibits increased Aβ phagocytic capacity will provide insight into the mechanisms underlying the IL-33–stimulated clearance of Aβ. In particular, recent identification of markers specific for resident microglia may facilitate further analysis of microglial regulation by IL-33 (38).

Direct degradation of Aβ by endopeptidases is another important pathway for its clearance (39). Exogenous expression of one of the enzymes, neprilysin, in the brains of AD transgenic mice causes a reduction of Aβ oligomers, the major species causing synaptotoxicity (40), whereas reducing the activity of neprilysin in the APP/$neprilysin^{-/-}$ double transgenic mice results in accumulation of Aβ, specifically the oligomeric form (41). The increase of neprilysin protein in the brains of APP/PS1 mice after IL-33 administration (Fig. 4 *A* and *B*) provides insight into the mechanism of the enzymatic degradation of Aβ in the IL-33–treated condition.

On exposure to Aβ during the progression of AD, microglia are converted into proinflammatory and activated phenotypes. Activated microglia result in Aβ accumulation by enhancing the production of Aβ peptides and reducing its phagocytosis and degradation (22). Along with recruiting monocytes to lesion sites, IL-33 acts as an alarmin for the polarization of macrophages toward the alternative phenotype after CNS injury (42). Indeed, we show that IL-33 administration causes an increase in the antiinflammatory genes Arg1 and Fizz1 in microglia/macrophages in the brain, suggesting that IL-33 enhances the polarization of microglia/macrophages to an alternative activation phenotype.

How does IL-33 modulate the functions of microglia/macrophages? Toll-like receptors (TLRs), including TLR2 and TLR4, have been identified as innate pattern recognition receptors that mediate the proinflammatory response (43, 44). TLR signaling via the adaptor protein MyD88 mediates inflammatory responses, such as inducing microglial phagocytic activity in early stages of inflammation and increasing transcription of genes encoding IL-1 family cytokines (44, 45). Indeed, inhibition of TLR2 or TLR4 reduces Aβ-stimulated microglial production of IL-1β and IL-6 (46, 47). IL-33/ST2 signaling acts as a negative regulator of TLR signaling by competing with MyD88 (48, 49). Specifically, ST2 activation recruits MyD88, which leads to MAPK activation for gene transcription (10). Whether this mechanism mediates the suppression of proinflammatory gene production in IL-33–treated APP/PS1 mice awaits further study.

It is tempting to speculate that relatively high levels of IL-33 in the CNS of healthy individuals (50) may be a key innate factor that protects against AD. The breakdown of this fail-safe mechanism owing to genetic disposition or environmental pressure thus may contribute to the onset of AD. Indeed, genetic studies have linked IL-33/ST2 single nucleotide polymorphisms to clinical AD (15, 51), suggesting that our observations in the murine AD model could be extrapolated to humans. Recent clinical trials of AD treatments have been unsuccessful, likely because the regimens aimed to bind monoclonal antibodies to Aβ or to prevent further Aβ accumulation at a late disease stage (52). Our finding that IL-33 mobilizes innate immunity to prevent and clear established Aβ accumulation even at late stages of the disease represents a new treatment paradigm for AD.

Methods

Reagents. Murine recombinant IL-33 was obtained from Biolegend (580506). sST2-Fc recombinant protein (1004-MR-050) and the ST2/IL-1 R4 Quantikine ELISA Kit (DST200) were purchased from R&D Systems. Antibodies specific for IL-33 (clone Nessy-1; ab54385) and APP (clone DE2B4; ab11132) were purchased from Abcam. Iba1 antibody (019-19741) was purchased from Wako; APC-conjugated antibody against CD11b (clone M1/70) and FITC-conjugated antibody against CD45 (clone 30-F11), from eBioscience; CD68 antibody (FA-11), from AbD Serotec; monoclonal 4G8 antibody (recognizes $A\beta_{17-24;}$ SIG-39220) for immunohistochemistry and 6E10 antibody (recognizes $A\beta_{1-16;}$ SIG-39320) for Western blot analysis, from Covance; insulin-degrading enzyme antibody (PC730), from Calbiochem; neprilysin antibody (H-321), from Santa Cruz Biotechnology; P-p38 (4511), p38 (9212), P-ERK1/2 (4377), and ERK1/2 (9102) antibodies, from Cell Signaling Technology; and actin antibody (clone AC-40; A4700), from Sigma-Aldrich. Fluorescein-beta-amyloid (1–42) (A-1119-1) was obtained from rPeptide; methoxy-X04 (4920), from Tocris Bioscience; DAB, from DAKO; Hoechst 34580 (H21486), human $A\beta_{x-40}$ (KHB3481), and $A\beta_{x-42}$ (KHB3441) commercial ELISA kits and Alexa Fluor secondary antibodies, from Life Technologies; and the histamine ELISA kit (ENZ-KIT140-0001), from Enzo Life Sciences.

Oligomeric Fluorescein-$A\beta_{1-42}$ Preparation. Monomeric $A\beta_{1-42}$ was dissolved in dry DMSO and diluted in ice-cold phenol red-free F-12 medium to a final concentration of 100 μM. The fluorescein-$A\beta_{1-42}$ solution was incubated at 4 °C for 24 h and then centrifuged at 14,000 × *g* for 10 min. The supernatant was frozen in liquid nitrogen as aliquots and stored at −20 °C for up to 1 mo (18).

Human Subjects. All cases involved Han Chinese patients. Clinical diagnosis was established according to criteria published by the National Institute of Neurological and Communicative Disorders and Stroke/Alzheimer's Disease and Related Disorders Association (2). The cases of MCI were gathered from outpatient or inpatient clinics at the Department of Neurology, Second Affiliated Hospital of the Zhejiang University School of Medicine, and the control group without dementia was recruited from the Health Examination Center between 2014 and 2015.

Data on age, sex, education, medical history, and family history were recorded as well (*SI Appendix*, Table S1). The sera of 17 healthy controls (NC) and 18 patients of mixed sex with MCI were collected. All of the NC and patients with MCI recruited were age ≥60 y. Patients with other neurologic or psychiatric disorders or clinically significant medical conditions were excluded. No patient had a history of head trauma or alcohol or drug abuse. This study was approved by the Institutional Ethics Committees of the Second Affiliated Hospital of the Zhejiang University School of Medicine and The Hong Kong University of Science and Technology (HKUST). Informed consent for participation in this study was obtained either directly or from a legal guardian.

Mice. The APP/PS1 double-transgenic mice, generated by incorporating a human/murine APP construct bearing the Swedish double mutation and the exon-9–deleted PSEN1 mutation (APPswe + PSEN1/dE9) (16), were obtained from the Jackson Laboratory (B6C3-Tg[APPswe, PSEN1dE9]85Dbo/J). The generation of 5XFAD mice overexpressing the K670N/M671L (Swedish), I716V (Florida), and V717I (London) mutations in human APP (695), as well as M146L and L286V mutations in human PS1, has been described previously (53). The 5XFAD mice were kindly provided by Sookja Kim Chung, The University of Hong Kong, Pokfulam, Hong Kong. The $St2^{-/-}$ mice were obtained from Andrew McKenzie, University of Cambridge, Cambridge, United Kingdom (54). Genotypes were confirmed by PCR analysis of tail or ear biopsy specimens. WT C57BL/6 mice were obtained from Jackson Laboratory.

All mice were housed in the HKUST Animal and Plant Care Facility, and all animal experiments were approved by the HKUST Animal Ethics Committee. Mice of the same sex were housed four per cage with a 12-h light/dark cycle and food and water ad libitum. All in vivo experiments were performed on sex- and age-matched groups. Mice of both genders were used for experiments. The mice were assigned at random to the experimental conditions. Sample sizes were chosen primarily on the basis of experience with similar types of experiments. All of the animal experiments were conducted in the light phase.

In Vivo Experiments. Murine recombinant IL-33 (200 ng per mouse) was injected i.p. into 6- to 25-mo-old mice. For studies of amyloid plaque load, microglial phagocytosis of Aβ, mRNA expression, and LTP, mice were injected with IL-33 for 2 consecutive days. The field excitatory postsynaptic potentials were recorded using a MED64 multichannel recording system (Panasonic International). For behavioral tests, mice were injected i.p. with IL-33 as indicated in Fig. 1 *D* and *E*. The open field test and contextual fear conditioning were conducted as described previously (55, 56). Soluble ST2 (sST2) was delivered into APP/PS1 mice via mini-osmotic pumps (model 1004; Alzet) at 0.11 μL/h. The min-iosmotic pumps were adjusted intracerebroventricularly in the right hemisphere. The pumps were loaded with murine recombinant sST2 protein (240 ng per pump; 10 μg/mL) or with vehicle in artificial cerebrospinal fluid (aCSF; 119 mM NaCl, 2.5 mM KCl, 2.5 mM $CaCl_2{\cdot}2H_2O$, 1 mM $NaH_2PO_4{\cdot}2H_2O$, 1.3 mM $MgCl_2{\cdot}6H_2O$, 26.2 mM $NaHCO_3$, 11 mM D-glucose). After 2 d of sST2 delivery, IL-33 was administered i.p. to mice for another 2 d. At the end of the treatment, the mice were killed and their brains fixed with 4% paraformaldehyde.

LTP. In brief, after the mice were killed, whole brains were immediately resected and soaked in ice-cold aCSF supplemented in 95% O_2/5% CO_2. Brain slices (300 μm) were then prepared using a vibratome (HM650V; Thermo Fisher Scientific) and soaked in oxygenated aCSF for 2 h at 32 °C. The mouse hippocampal slices were placed on a precoated polyethylenimine (Sigma-Aldrich) on a MED–P210A probe (Panasonic International) fabricated with 8 × 8 electrode arrays (20 × 20 μm, indium tin oxide and platinum black) with a 100-μm interelectrode distance. Electrodes were manually placed at the CA3–CA1 region under a microscope (MIC-D; Olympus). Each slice was submerged in and superfused with oxygenated aCSF at 1.3–1.5 mL/min.

Field excitatory postsynaptic potentials (fEPSPs) were recorded from the dendritic layer of CA1 neurons by selecting an electrode in the Schaffer collateral pathway as the stimulating electrode. Based on the stimulus–response curve, a stimulation intensity that evoked an fEPSP with 30–40% of the maximum response was selected. LTP was induced by three trains of high-frequency stimulation (100 Hz for 1 s, delivered 30 s apart). The field potential response after the tetanus was recorded for 60 min. The magnitude of LTP was quantified as the percentage change in the average slope of the fEPSP over 60 min after LTP induction (18).

Open Field Test. The locomotor activity of the mice in the open field test was recorded and tracked using a photobeam activity system and software (San Diego Instruments). In brief, experimental mice were placed in the center of an open-top chamber (16 × 16 × 15 inches) with an array of photobeams around the periphery. The mice were allowed to explore the chamber for 15 min each day for 3 consecutive days. Locomotor activity in the three training trials was recorded by the photobeams, and the distance moved was subsequently determined. The chamber was cleaned with 70% ethanol after each trial.

Contextual Fear Conditioning. On the day of training, the mice were allowed to explore in an enclosed training chamber with the floor wired to an electric shock generator for 180 s. The mice were then exposed to a pure tone for 30 s, followed by a 2-s foot shock (0.8 mA). At 60 s after delivery of the second shock, the mice were returned to their home cages. The fear response (freezing) was assessed at 1 d and 7 d after the electric shock. The mice were re-exposed in the original chamber for 5 min, and the time of freezing was measured using the Contextual NIR Video Fear Conditioning System (Med Associates).

Immunohistochemistry. Coronal cryosections (20 μm) of perfused mouse brains were used for immunohistochemistry. For 4G8 immunostaining, antigen retrieval was performed by microwave heating of the sections in sodium citrate buffer (10 mM trisodium citrate, 0.5% Tween-20 in H_2O, pH 6.0) for 10 min, followed by incubation with 3% H_2O_2 in H_2O for 5 min to inhibit

endogenous peroxidase activity. The sections were blocked with 2% goat serum in Tris-buffered saline for 20 min and then labeled with 4G8 antibody (dilution 1:500) in blocking buffer overnight at 4 °C. The sections were then labeled with a Dako HRP-linked goat anti-mouse/rabbit IgG antibody for 50 min at room temperature and developed with a Dako DAB chromogen kit.

Imaging was performed using a Leica DM6000 B compound microscope system. The area of Aβ plaques in the cortex of the brain sections was analyzed by the "Analyze Particles" function of ImageJ. The region of the cortex used for amyloid plaque analysis was above the hippocampus. Three brain sections per mouse (~200–300 μm apart) were analyzed, and the average percentage of cortical area occupied by amyloid plaques was calculated.

To examine the colocalization of amyloid plaques and microglia, the brain sections were blocked with 1% BSA, 4% goat serum, and 0.4% Triton X-100 in Dulbecco's PBS (DPBS) for 30 min at room temperature and then incubated with Iba1 (1:500 dilution) and 4G8 (1:1,000 dilution) antibodies overnight at 4 °C. Imaging was performed using a Leica TCS SP8 confocal system. Quantification of the 3D-colocalization was conducted using the Imaris software (Bitplane).

To determine the blood–brain barrier penetrability of IL-33, 11-mo-old APP/PS1 mice were injected i.p. with IL-33 (200 ng) in DPBS or DPBS alone. Mouse cortices and sera were collected for IL-33 ELISA.

Aβ Extraction, Western Blot Analysis, and ELISA. Aβ was sequentially extracted from the soluble and insoluble fractions of the mouse cortex (16, 18). Frozen brain tissues were lysed in indicated lysis buffers with various protease inhibitors (18). In brief, the mouse cortex was homogenized in buffer containing 250 mM sucrose, 20 mM Tris·HCl pH 7.4, 1 mM EDTA, 1 mM EGTA, and protease inhibitor mixture (Sigma-Aldrich) or in radioimmunoprecipitation assay buffer. Densitometric quantification of protein band intensity from Western blot analysis was performed using ImageJ. Soluble Aβ was sequentially extracted by diethylamine (soluble), followed by formic acid (insoluble). Levels of soluble and insoluble Aβ were determined by Western blot analysis. Soluble $A\beta_{x-40}$ and $A\beta_{x-42}$ were analyzed by ELISA.

Isolation of Mouse Microglia. Adult mice were anesthetized and perfused with ice-cold DPBS. The isolated forebrain were cut into small pieces and dissociated enzymatically and mechanically using a papain-based neural dissociation kit (130-092-634; Miltenyi Biotec) with a gentleMACS dissociator system (Miltenyi Biotec) according to the manufacturer's instructions. Percoll gradient (30%; Sigma-Aldrich) was used to remove myelin. The resultant mononuclear cell suspensions were used for flow cytometry analysis or for preparation of microglial cultures (57). The purity of microglia/infiltrating monocyte isolation was routinely >90% as determined by fluorescence staining for CD11b and flow cytometry analysis.

Analysis of Microglial Phagocytosis of Aβ. For in vivo analysis, the experiment was performed as described previously (29). APP/PS1 or WT mice (17 mo old) were injected i.p. with IL-33 in PBS or PBS alone daily for 2 consecutive days. The next day, the mice were injected i.p. with methoxy-X04 (10 mg/kg). The mice were deeply anesthetized at 3 h after methoxy-X04 injection and perfused in the left ventricle with ice-cold PBS. Isolated mononuclear cell suspensions from the mouse forebrain were then incubated with a mouse FcR blocking reagent (Miltenyi Biotec) and labeled with APC-conjugated mouse CD11b (1:100 dilution) and FITC-conjugated CD45 (1:100 dilution) antibodies and analyzed using a BD FACSAria IIIu flow cytometer. Myeloid cells were identified as $CD11b^+$ cells and were further classified as microglia or infiltrating monocytes based on low ($CD11b^+CD45^{lo}$) or high ($CD11b^+CD45^{hi}$) CD45 expression, respectively (29).

For the in vitro microglial phagocytosis assay, microglia cells were prepared from $St2^{+/+}$ or $St2^{-/-}$ mice (1.5 to 2 mo old) and cultured for 6–7 d in vitro. The cells were then pretreated with IL-33 for 20 h, followed by fluorescein-$A\beta_{1-42}$ (2 μM) for 1 h. The cells were then fixed with paraformaldehyde and immunostained with Iba1 antibody and Hoechst 34580. Wide-field fluorescence microscopy was performed using an IN Cell Analyzer 6000 system (GE Healthcare). Images were acquired at 16 corresponding positions assigned by the software in each well. Intensity segmentation was applied to each channel using the same thresholding criteria across different samples. The boundaries of microglia were determined according to $Iba1^+$ labeling intensity, and fluorescein-$A\beta_{1-42}$ in each $Iba1^+$ cell was quantified. The area of phagocytosed fluorescein-$A\beta_{1-42}$ was divided by the corresponding cell area to obtain the relative area of fluorescein-$A\beta_{1-42}$ in a given cell.

Droplet Digital PCR and qRT-PCR. For droplet digital PCR (ddPCR), RNA from mouse cortices was extracted using TRIzol (Invitrogen) and the RNeasy Mini Kit (Qiagen) and quantified using a BioDrop μLITE microvolume spectrophotometer. Equivalent amounts of RNA were reverse-transcribed using the PrimeScript RT-PCR Kit (TaKaRa). ddPCR was performed according to the manufacturer's protocol (Bio-Rad). The copy numbers for samples were averaged across duplicates. The copy numbers of target genes were normalized to those of GAPDH or β-actin.

For qRT-PCR, cDNA after reverse transcription was preamplified using TaqMan PreAmp Master Mix (Invitrogen). The PCR amplification and real-time detection of PCR products were performed using TaqMan gene expression assay (Applied Biosystems) and Premix Ex Taq qPCR assay (TaKaRa). PCR analyses were conducted in a total volume of 20 μL containing 2 μL of preamplified product. The mRNA expression values were normalized to the level of β-actin, GAPDH, or CD11b as indicated. The following TaqMan probes were used: NLRP3 (Mm00840904_m1), IL-1β (Mm01336189_m1), IL-6 (Mm00446190_m1), IL-13 (Mm00434204_m1), TGFβ (Mm01178820_m1), GAPDH (Mm99999915_g1), β-actin (Mm02619580_g1), ST2 total (Mm00516117_m1), Fizz1 (Mm00445109_m1), Arg1 (Mm00475988_m1), and CD11b (Mm00434455_m1).

Statistical Analysis. The investigators who performed the electrophysiological, immunohistochemical, RNA expression, and flow cytometry analyses and the behavioral tests were blinded to the genotypes of the mice and treatment conditions. All data are expressed as arithmetic mean ± SEM, except for human sST2 serum level. All statistical analyses were performed using GraphPad Prism version 6.0. The significance of differences was assessed by the unpaired Student's *t* test or one- or two-way ANOVA followed by the Bonferroni post hoc test as indicated. The level of significance was set at $P < 0.05$. Soluble ST2 levels were recorded for NC subjects and patients with MCI, with data analyses performed using R version 3.2.2. The Shapiro–Wilk test was used to assess the normality of the continuous measurements. Statistical comparisons of ST2 levels in the two subject groups were compared using a two-sample *t* test.

ACKNOWLEDGMENTS. We thank Dr. Yu Chen, Dr. Yang Shen, Dr. Fanny C. F. Ip, Dr. Terry C. T. Or, Estella P. S. Tong, Elaine Y. L. Cheng, Minty M. Tian, Kit Cheung, Fion C. Y. Chuang, and William Chau for their excellent technical assistance; Dr. Maggie M. K. Chu for statistical analysis; and members of the N.Y.I. laboratory for many helpful discussions. We also thank Dr. Sookja Kim Chung for the 5XFAD mice, Dr. Richard Ransohoff for expert advice on the preparation and isolation of microglia, and Drs. Karl Herrup and Gary Landreth for helpful discussions. This study was supported in part by the Research Grants Council of Hong Kong SAR (C6003-14G), the National Key Basic Research Program of China (2013CB530900), a Hong Kong Research Grants Council Theme-based Research Scheme (T13-607/12R), and the S. H. Ho Foundation.

1. Alzheimer's Association (2015) 2015 Alzheimer's disease facts and figures. *Alzheimers Dement* 11(3):332–384.
2. McKhann G, et al. (1984) Clinical diagnosis of Alzheimer's disease: Report of the NINCDS-ADRDA Work Group under the auspices of the Department of Health and Human Services Task Force on Alzheimer's Disease. *Neurology* 34(7): 939–944.
3. Carrillo MC, et al. (2013) Revisiting the framework of the National Institute on Aging–Alzheimer's Association diagnostic criteria. *Alzheimers Dement* 9(5):594–601.
4. Tanzi RE (2012) The genetics of Alzheimer disease. *Cold Spring Harb Perspect Med* 2(10):a006296.
5. Heppner FL, Ransohoff RM, Becher B (2015) Immune attack: The role of inflammation in Alzheimer disease. *Nat Rev Neurosci* 16(6):358–372.
6. Vom Berg J, et al. (2012) Inhibition of IL-12/IL-23 signaling reduces Alzheimer's disease-like pathology and cognitive decline. *Nat Med* 18(12):1812–1819.
7. Heneka MT, et al. (2013) NLRP3 is activated in Alzheimer's disease and contributes to pathology in APP/PS1 mice. *Nature* 493(7434):674–678.
8. Guillot-Sestier M-V, et al. (2015) Il10 deficiency rebalances innate immunity to mitigate Alzheimer-like pathology. *Neuron* 85(3):534–548.
9. Chakrabarty P, et al. (2015) IL-10 alters immunoproteostasis in APP mice, increasing plaque burden and worsening cognitive behavior. *Neuron* 85(3):519–533.
10. Liew FY, Pitman NI, McInnes IB (2010) Disease-associated functions of IL-33: The new kid in the IL-1 family. *Nat Rev Immunol* 10(2):103–110.
11. Han P, Mi WL, Wang YQ (2011) Research progress on interleukin-33 and its roles in the central nervous system. *Neurosci Bull* 27(5):351–357.
12. Gadani SP, Walsh JT, Smirnov I, Zheng J, Kipnis J (2015) The glia-derived alarmin IL-33 orchestrates the immune response and promotes recovery following CNS injury. *Neuron* 85(4):703–709.
13. Yasuoka S, et al. (2011) Production and functions of IL-33 in the central nervous system. *Brain Res* 1385:8–17.
14. Molofsky AB, Savage AK, Locksley RM (2015) Interleukin-33 in tissue homeostasis, injury, and inflammation. *Immunity* 42(6):1005–1019.
15. Chapuis J, et al. (2009) Transcriptomic and genetic studies identify IL-33 as a candidate gene for Alzheimer's disease. *Mol Psychiatry* 14(11):1004–1016.

16. Jankowsky JL, et al. (2004) Mutant presenilins specifically elevate the levels of the 42 residue beta-amyloid peptide in vivo: Evidence for augmentation of a 42-specific gamma secretase. *Hum Mol Genet* 13(2):159–170.
17. Jacobsen JS, et al. (2006) Early-onset behavioral and synaptic deficits in a mouse model of Alzheimer's disease. *Proc Natl Acad Sci USA* 103(13):5161–5166.
18. Fu AK, et al. (2014) Blockade of EphA4 signaling ameliorates hippocampal synaptic dysfunctions in mouse models of Alzheimer's disease. *Proc Natl Acad Sci USA* 111(27): 9959–9964.
19. Minogue AM, et al. (2014) Age-associated dysregulation of microglial activation is coupled with enhanced blood-brain barrier permeability and pathology in APP/PS1 mice. *Neurobiol Aging* 35(6):1442–1452.
20. Montagne A, et al. (2015) Blood-brain barrier breakdown in the aging human hippocampus. *Neuron* 85(2):296–302.
21. Mucke L, Selkoe DJ (2012) Neurotoxicity of amyloid β-protein: Synaptic and network dysfunction. *Cold Spring Harb Perspect Med* 2(7):a006338.
22. Malm TM, Jay TR, Landreth GE (2015) The evolving biology of microglia in Alzheimer's disease. *Neurotherapeutics* 12(1):81–93.
23. Gomez-Nicola D, Perry VH (2015) Microglial dynamics and role in the healthy and diseased brain: A paradigm of functional plasticity. *Neuroscientist* 21(2):169–184.
24. Wang Y, et al. (2015) TREM2 lipid sensing sustains the microglial response in an Alzheimer's disease model. *Cell* 160(6):1061–1071.
25. Yamada Y, Doi T, Hamakubo T, Kodama T (1998) Scavenger receptor family proteins: Roles for atherosclerosis, host defence and disorders of the central nervous system. *Cell Mol Life Sci* 54(7):628–640.
26. de Villiers WJ, Smart EJ (1999) Macrophage scavenger receptors and foam cell formation. *J Leukoc Biol* 66(5):740–746.
27. Derecki NC, Katzmarski N, Kipnis J, Meyer-Luehmann M (2014) Microglia as a critical player in both developmental and late-life CNS pathologies. *Acta Neuropathol* 128(3): 333–345.
28. Zhou X, He X, Ren Y (2014) Function of microglia and macrophages in secondary damage after spinal cord injury. *Neural Regen Res* 9(20):1787–1795.
29. Zhang GX, Li J, Ventura E, Rostami A (2002) Parenchymal microglia of naïve adult C57BL/6J mice express high levels of B7.1, B7.2, and MHC class II. *Exp Mol Pathol* 73(1): 35–45.
30. Malito E, Hulse RE, Tang WJ (2008) Amyloid beta-degrading cryptidases: Insulin-degrading enzyme, presequence peptidase, and neprilysin. *Cell Mol Life Sci* 65(16): 2574–2585.
31. Heneka MT, et al. (2015) Neuroinflammation in Alzheimer's disease. *Lancet Neurol* 14(4):388–405.
32. Ousman SS, Kubes P (2012) Immune surveillance in the central nervous system. *Nat Neurosci* 15(8):1096–1101.
33. McLaren JE, et al. (2010) IL-33 reduces macrophage foam cell formation. *J Immunol* 185(2):1222–1229.
34. Miller AM, et al. (2008) IL-33 reduces the development of atherosclerosis. *J Exp Med* 205(2):339–346.
35. Stewart CR, et al. (2010) CD36 ligands promote sterile inflammation through assembly of a Toll-like receptor 4 and 6 heterodimer. *Nat Immunol* 11(2):155–161.
36. Mawuenyega KG, et al. (2010) Decreased clearance of CNS beta-amyloid in Alzheimer's disease. *Science* 330(6012):1774.
37. Hickman SE, Allison EK, El Khoury J (2008) Microglial dysfunction and defective beta-amyloid clearance pathways in aging Alzheimer's disease mice. *J Neurosci* 28(33): 8354–8360.
38. Bennett ML, et al. (2016) New tools for studying microglia in the mouse and human CNS. *Proc Natl Acad Sci USA* 113(12):E1738–E1746.
39. Miners JS, Barua N, Kehoe PG, Gill S, Love S (2011) Aβ-degrading enzymes: Potential for treatment of Alzheimer disease. *J Neuropathol Exp Neurol* 70(11):944–959.
40. Iwata N, et al. (2013) Global brain delivery of neprilysin gene by intravascular administration of AAV vector in mice. *Sci Rep* 3:1472.
41. Huang SM, et al. (2006) Neprilysin-sensitive synapse-associated amyloid-beta peptide oligomers impair neuronal plasticity and cognitive function. *J Biol Chem* 281(26): 17941–17951.
42. Gadani SP, Walsh JT, Lukens JR, Kipnis J (2015) Dealing with danger in the CNS: The response of the immune system to injury. *Neuron* 87(1):47–62.
43. Wada J, Makino H (2016) Innate immunity in diabetes and diabetic nephropathy. *Nat Rev Nephrol* 12(1):13–26.
44. O'Neill LA, Golenbock D, Bowie AG (2013) The history of Toll-like receptors: Redefining innate immunity. *Nat Rev Immunol* 13(6):453–460.
45. Neher JJ, et al. (2011) Inhibition of microglial phagocytosis is sufficient to prevent inflammatory neuronal death. *J Immunol* 186(8):4973–4983.
46. Jana M, Palencia CA, Pahan K (2008) Fibrillar amyloid-beta peptides activate microglia via TLR2: Implications for Alzheimer's disease. *J Immunol* 181(10):7254–7262.
47. Costello DA, Carney DG, Lynch MA (2015) α-TLR2 antibody attenuates the Aβ-mediated inflammatory response in microglia through enhanced expression of SIGIRR. *Brain Behav Immun* 46:70–79.
48. Liu J, Buckley JM, Redmond HP, Wang JH (2010) ST2 negatively regulates TLR2 signaling, but is not required for bacterial lipoprotein-induced tolerance. *J Immunol* 184(10):5802–5808.
49. Brint EK, et al. (2004) ST2 is an inhibitor of interleukin 1 receptor and Toll-like receptor 4 signaling and maintains endotoxin tolerance. *Nat Immunol* 5(4):373–379.
50. Schmitz J, et al. (2005) IL-33, an interleukin-1-like cytokine that signals via the IL-1 receptor-related protein ST2 and induces T helper type 2-associated cytokines. *Immunity* 23(5):479–490.
51. Yu JT, et al. (2012) Implication of IL-33 gene polymorphism in Chinese patients with Alzheimer's disease. *Neurobiol Aging* 33(5):1014.e11–1014.e14.
52. Spencer B, Masliah E (2014) Immunotherapy for Alzheimer's disease: Past, present and future. *Front Aging Neurosci* 6:114.
53. Oakley H, et al. (2006) Intraneuronal beta-amyloid aggregates, neurodegeneration, and neuron loss in transgenic mice with five familial Alzheimer's disease mutations: Potential factors in amyloid plaque formation. *J Neurosci* 26(40):10129–10140.
54. Xu D, et al. (2008) IL-33 exacerbates antigen-induced arthritis by activating mast cells. *Proc Natl Acad Sci USA* 105(31):10913–10918.
55. Sananbenesi F, et al. (2007) A hippocampal Cdk5 pathway regulates extinction of contextual fear. *Nat Neurosci* 10(8):1012–1019.
56. Ip FC, et al. (2015) Anemoside A3 enhances cognition through the regulation of synaptic function and neuroprotection. *Neuropsychopharmacology* 40(8):1877–1887.
57. Nikodemova M, Watters JJ (2012) Efficient isolation of live microglia with preserved phenotypes from adult mouse brain. *J Neuroinflammation* 9:147.